Development and Integration of a Thermal Management Simulation for a Quadrotor Parallel Hybrid Propulsion System

Jeffryes W. Chapman*, George L. Thomas†, Brian P. Malone‡
NASA Glenn Research Center, Cleveland, OH, 44135, USA

This paper details the development of a propulsion system simulation for a six-passenger parallel hybrid quadrotor and utilizes the Numerical Propulsion System Simulation (NPSS) along with the NPSS Power System Library as the development environment. This simulation integrates an engine power plant with an electrical generation and distribution system and includes the required thermal management system. The thermal management system is comprised of liquid cooling loops that reject the heat load through air-to-coolant heat exchangers, and utilizes a map-based performance estimation method. This method is developed within NPSS and detailed in this paper. The full system model is designed to predict system weight, range, and performance through a proposed mission profile. Results of the paper show an all-engine system maintains the best range, while a mostly electric system that utilizes an engine as a backup or a conditional power contributor offers range benefit.

Nomenclature

A	Heat transfer area
AU	Heat transfer area * Overall heat transfer coefficient
$AUqV$	AU/V
C	Heat capacity rate, $C = C_p * \dot{m}$
C_p	Specific heat at constant pressure
CR	Heat capacity rate ratio
D_{climb}	Climb distance
dP	Change in pressure
EAP	Electrified aircraft propulsion
h	Heat transfer coefficient
ht	Total enthalpy
ISA	International standard atmosphere
MSL	Mean sea level
$\dot{m}$	Mass flow
NPSS	Numerical Propulsion System Simulation
NTU	Number of Transfer Units
P	Pressure
P_{climb}	Climb power
P_{cruise}	Cruise power
Q	Heat transfer rate
ROC	Rate of climb
SLS	Sea level static conditions
T	Temperature
t	time

* Research Engineer, 21000 Brookpark Rd., Cleveland, OH, MS-5-11, jeffryes.w.chapman@nasa.gov.
† Research Engineer, 21000 Brookpark Rd., Cleveland, OH, MS-301-5, george.l.thomas@nasa.gov.
‡ Research Engineer, 21000 Brookpark Rd., Cleveland, OH, MS-301-5, brian.p.malone@nasa.gov.

U	Overall heat transfer coefficient
V	Volume
V_{br}	Best range speed
V_y	Vertical speed
η_o	Overall fin effectiveness
α	heat exchanger heat transfer area on one surface to total volume, $\frac{A_{th}}{V}$
ε	Effectiveness
ρ	Density

Subscripts

c	Cold surface
h	Hot surface
in	Input
max	Maximum
min	Minimum
out	Output
th	Thermal

I. Introduction

Interest in urban air mobility (UAM) vehicles with electric aircraft propulsion (EAP) systems has been increasing over the last decade [1]. Contributing to this interest, the NASA Aeronautics Research Mission Directorate has pursued UAM technologies as part of the "Safe, Quiet, and Affordable Vertical Lift Air Vehicles" strategic thrust. To meet this goal, NASA has also developed concept vehicles to showcase promising technologies [2]. Of these concepts, electric vertical take-off and landing (eVTOL) vehicles have been developed to meet the potential of an UAM mission [3][4]. This paper details the design of a parallel hybrid EAP system for one such eVTOL vehicle. This multidisciplinary simulation consists of electrical power, engine, thermal management system (TMS), and propulsor sub-systems. Modeling methods use the Numerical Propulsion System Simulation (NPSS) default components for the engine [5], the NPSS Power System Library (NPSL) for the electrical system [6][7], and custom thermal management components for the heat rejection system. Theory for these TMS components will be detailed within this paper.

Originally developed by NASA, the NPSS software is a modular framework created to simulate multidisciplinary systems. This software has historically been used to develop models of gas turbine engines, however the framework is flexible enough to facilitate the development of larger scale system models. As EAP systems have become more common, there has been interest in developing electric powertrain models utilizing NPSS. The NPSL was developed to address this goal. The NPSL makes use of the new NPSS electric port to develop the required electric powertrain, which includes components such as wires, motors, motor drivers, and batteries that may utilize DC, AC, or 3-phase power distribution systems. The TMS required for cooling the electrical components offers the third major discipline in an EAP system design. Simulation of the TMS utilizes custom NPSS components.

Work within this paper is a continuation of previous studies and development detailed within Ref. [8]. In these studies, four powertrain architecture designs were completed on a six-passenger quadrotor vehicle intended for a UAM mission. The powertrains studied included a DC all-electric system, a DC all-electric with AC secondary system, a turboelectric, and a DC series hybrid. Each powertrain was tuned to maximize range while maintaining a design weight dictated by the described vehicle model, Ref. [3]. The electrical hardware was selected to meet power requirements, then fuel or battery capacity was added to meet the baseline powertrain weight. Range was determined with powertrain efficiency and the onboard fuel or battery capacity. The study within this paper will expand on these results with a DC parallel hybrid powertrain and additional TMS modeling details.

Subsequent sections of this paper detail the EAP system, review TMS modeling methods, and perform sensitivity studies on degree of hybridization and several other powertrain configurations. Specifically, a review of TMS simulation methods is shown in Section II. Details of the vehicle model and mission profile is given in Section III. System study results are then found in Section IV. Finally, summary and conclusions are given in Section V.

II. Thermal Management System Modeling

A liquid based TMS strategy is employed within this paper. In these systems, a liquid coolant gathers the heat loads then rejects that heat to air through a liquid to air heat exchanger. System components include heat exchangers, coolant tubing, pumps, ducting, puller fans, and air network exhaust nozzles. Default NPSS contains many elements and capabilities that naturally fit this type of simulation, though some of these need to be updated or worked around to meet modeling requirements. Figure 1 shows a simple TMS for a single load with coolant fluid drawn with a pump on the load side and an inlet nozzle with air drawn by a puller fan into an exhaust nozzle on the air side of the system. This system can be broken into two parts, the air side portion and the coolant side portion of the model. The air side includes the inlet, air side of the heat exchanger, puller fan and nozzle. The coolant side includes the heat rejection system of the load, a coolant pump, and the coolant side of the heat exchanger. The heat exchanger in the system acts to transfer the heat from the coolant and place it into the air. For this project it was determined that the default inlet, puller fan (compressor), and nozzle elements within NPSS are satisfactory for the performance modeling effort. For the heat exchanger, load, and pump element, modifications were required. Techniques for these adjustments are based on previous work and development of a TMS modeling Python code, which is detailed in Ref. [9]. In studying the previous work, it can be noticed that some of the elements will be done as in Ref. [9]., but some are modeled differently. Differences are detailed within this section.

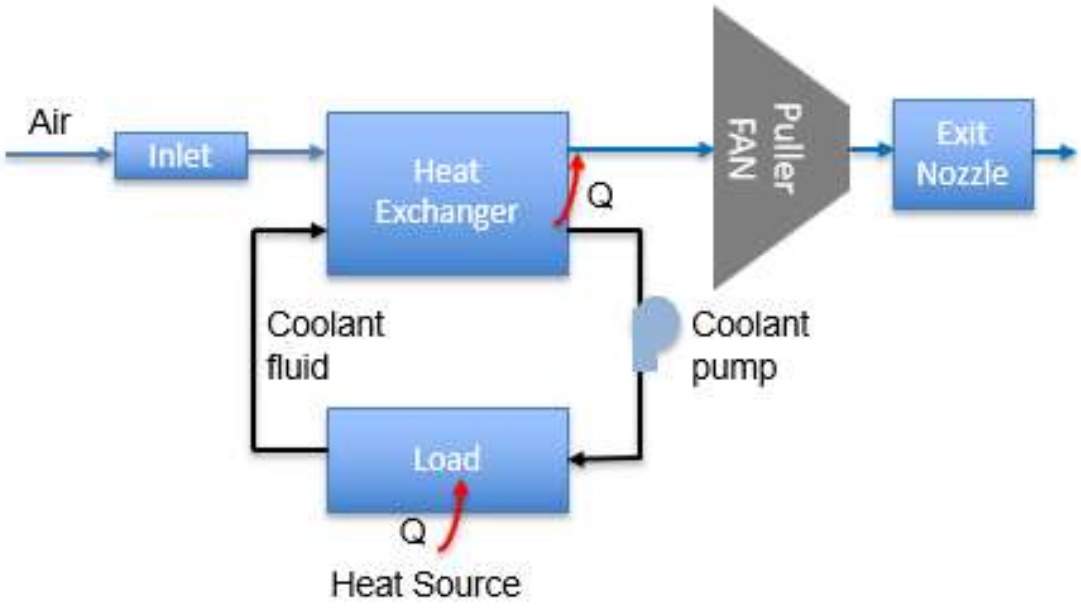

Figure 1. Example thermal management system archetecture.

Model setup must be addressed when creating a TMS system model within NPSS. In NPSS, flow properties are determined by a thermodynamics package. Elements within NPSS must use a single thermodynamic package for all flows defined within that element. This means that the air side and coolant side of a heat exchanger must be managed by the same NPSS thermodyanamics package. When modeling a TMS system it is desirable to utilize a baseline thermodynamics package for the air side as there are many options for this. However, in the baseline NPSS package there is not an option for many liquid coolants, which leads to them being defined with NPSS fluid property tables (FPT). This discrepancy leads to the heat exchanger requiring two thermal packages. As a work around the air thermal package can be updated to FPT before the heat exchanger element is called and the element can utilize only the FPT thermal package. Once the element has completed running the thermal package may be changed back to the desired type. Because thermal package is inherited, for each of these transitions flowEnd and flowStart elements will need to be added before and after each of these transitions. These elements must inherit the pressures and temperatures of the upstream elements. Syntax for this type of transition for air is shown in Figure 2.

```
Element FlowEnd fe_air{}

setThermoPackage("FPT");
Element FlowStart fs_air2{
  void preexecute(){
     W = fe_air.Fl_I.W;
     Tt = fe_air.Fl_I.Tt;
     Pt = fe_air.Fl_I.Pt;
   }
}
```

Figure 2. Example NPSS thermal package transition.

The coolant pump element is modeled identically here as it was within the Python code in Ref. [9] but will be discussed for completeness. Power required to run the coolant pump is calculated as a function of pressure drop as shown in Eq. (1), where P is pressure, ρ is density, and $\dot{m}$ is mass flow. Pump weight is calculated based on the flow requirement and using the empirical correlations, as shown in Eqns. (2) and (3), where mass flow is in lbm/s, density is in lbm/in.^{3}, pump displacement is in in.^{3}/rev, and weight is in lbm. Coolant piping models utilize the NPSS duct elements with assumed pressure drops.

$$Power_{pump} = \frac{\dot{m} * \Delta P}{\rho} \tag{1}$$

$$PumpDisplacment = 0.0092 * \left(\frac{\dot{m}_{coolant}}{\rho_{coolant}}\right)^{1.3857} \tag{2}$$

$$Weight_{pump} = 8.5942 * PumpDisplacement + 2.4229 \tag{3}$$

The heat load in NPSS is handled in two steps, determining heat transfer from the load to the flow and solving for the electrical surface temperature. To make a uniform modeling solution for many load cooling structures, it uses a constant effectiveness (ε) and pressure drop (dP) method to solve for the heat transfer into the system as shown in Eqns. (4) to (6), where Q is heat transfer rate, C_p is specific heat at constant pressure, T is temperature, and P is pressure. Once pressure drop and heat transfer rate have been calculated, properties for the coolant flow can be updated utilizing the total enthalpy (ht) , shown in Eq. (7), and output pressure, along with the NPSS method setTotal_hP, to populate the flow properties structure. Surface temperature is calculated based on a heat transfer integration as shown in Eq. (8), where dt is the time step and dT is the change in temperature.

$$Q_{max,coolant} = \dot{m}_{coolant} * C_{p,in,coolant} * \left(T_{component} - T_{in,coolant}\right) \tag{4}$$

$$Q_{coolant} = \varepsilon * Q_{max,coolant} \tag{5}$$

$$P_{out,coolant} = P_{in,coolant} - dP \tag{6}$$

$$ht_{out,coolant} = ht_{in,coolant} + \frac{Q_{coolant}}{\dot{m}_{coolant}} \tag{7}$$

$$\frac{dT_{component}}{dt} = \frac{Q_{component} - Q_{coolant}}{m_{component} * C_{p,component}} \tag{8}$$

The heat exchanger element provides the transition of heat from the coolant to air, which results in a heat rejected from the system. Calculation of this transfer uses an effectiveness model and makes use of the number of transfer units (NTU) method [10] and heat exchanger surface maps that relate the $AUqV$ of each heat exchanger surface to the mass

flow and coolant temperature at that surface. A heat exchanger surface is defined as a side of the heat exchanger that flow is driven through, so for a heat exchanger that transfers heat from a coolant to air, there would be 2 surfaces (hot coolant side and a cold air side). The methods described here are different from Ref. [9], where a heat exchanger design was optimized for performance. Here, the maps assume a heat exchanger geometry and when the system is run on-design the heat exchanger will be scaled up to meet the heat load requirement. Advantages of the map method are that the calculations are simpler, the model does not depend on a specific surface definition (as defined by Kays and London [11]), and new surface maps can be developed empirically for next generation heat exchangers. Disadvantages of the map method are that the design is not easily updated for changes in load temperature requirements, environmental characteristics, or coolant fluid types. To illustrate this, the code developed in Ref. [9] was used to run rejected power sweeps, from 25 hp to 275 hp, for a series of heat exchanger designs. Results show AU and weight increase linearly and as a function of volume, as shown in Figure 3. It also shows the change in $AUqV$ deviation, where the red line utilizes the code from Ref. [9] and the blue line utilizes the map method, is less than 0.05% for the considered range of designs.

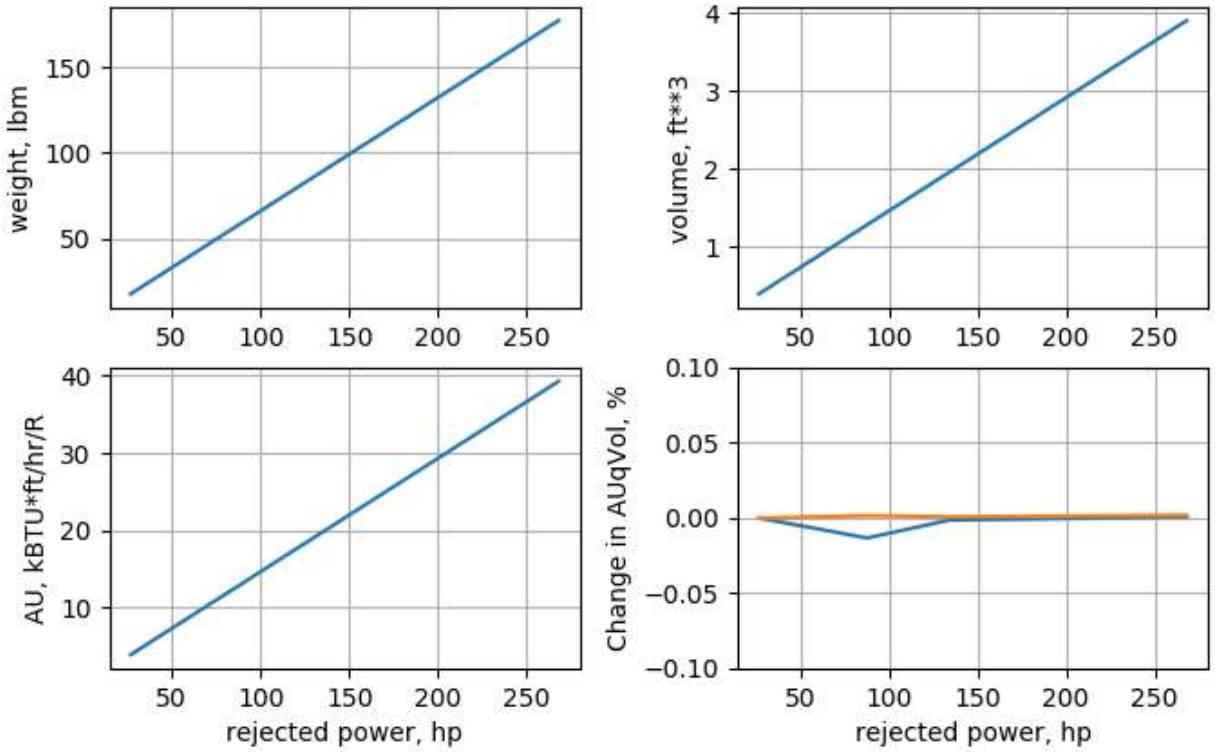

Figure 3. Heat exchanger design sensitivity to rejected power.

The method used for the map-based design is as follows. The relationship for AU is developed using a thermal network equation developed in equation 9 in Ref. [9]. This equation is also shown in Eq. (9), where A is area, U is overall thermal conductance, η_o is overall fin effectiveness, h is heat transfer coefficient, and α is the ratio of total heat transfer area to the total volume. The hot side thermal area to total volume is then multiplied through, resulting in Eq. (10), This equation can be reduced by dividing by total volume (V) and assuming $A_{th,h}U_h = A_{th,c}U_c = AU$, as shown in Eq. (11). The final map value for each surface look up is noted in Eq. (12) by replacing $\eta h \alpha$ with $AUqV$. Map $AUqV$ values are set as functions of fluid temperature and mass flow.

$$\frac{1}{U_h} = \frac{1}{\eta_{oh} h_h} + \frac{1}{\eta_{oc} h_c \frac{\alpha_c}{\alpha_h}} \tag{9}$$

$$\frac{1}{U_h \alpha_h} = \frac{1}{\eta_{oh} h_h \alpha_h} + \frac{1}{\eta_{oc} h_c \alpha_c} \tag{10}$$

$$\frac{1}{AU} = \frac{1}{\eta_{oh} h_h \alpha_h * V} + \frac{1}{\eta_{oc} h_c \alpha_c * V} \tag{11}$$

$$\frac{1}{AU} = \frac{1}{AUqV_h * V} + \frac{1}{AUqV_c * V} \tag{12}$$

Once AU has been obtained the NTU is calculated as shown in Eq. (13), where $C_{min}$is the minimum capacity rate of the two flows.

$$NTU = \frac{AU}{C_{min}} \tag{13}$$

With NTU the heat exchanger effectiveness is calculated based on the heat exchanger type, such as double pipe parallel flow, counter-flow, or crossflow all specified with an empirical function. A variety heat exchanger types can be found in Ref. [11]. This paper will assume a crossflow type heat exchanger with the relationship describe in Eq. (14), where $CR = \frac{C_{min}}{C_{max}}$, with C_{max} being the maximum capacity rate of the two flows.

$$\epsilon = 1 - \exp\left[\left(\frac{1}{CR}\right) NTU^{0.22}\{exp[-CR * NTU^{0.78}] - 1\}\right] \tag{14}$$

Once effectiveness is determined, the maximum Q across the heat exchanger is calculated as shown in Eq. (15). Final Q and coolant and air enthalpies are derived as previously defined in Eqns. (5) and (7).

$$Q_{max} = C_{min}\left(T_{h,in} - T_{c,in}\right) \tag{15}$$

With this map-based modeling, heat exchanger weight and pressure drop are determined empirically as functions of volume and mass flow, respectively. Final exit flow parameters are calculated utilizing the NPSS setTotal_hP method.

During on-design operation map placement is set using $AUqV$ design values and a design pressure drop, and scalars are set to match the map value with the design value. Off design, $AUqV$ varies with mass flow and temperature as the map specifies. The design scalar is applied to the off design $AUqV$ determined by the map to obtain the final value. Heat exchanger maps for this study were derived using the optimization design code detailed in Ref [9]. This map is detailed in the appendix.

III. Six Passenger Quadrotor

The vehicle selected for this study is a six-passenger quadrotor shown in Figure 4. System design details for this vehicle are within Ref. [3] and [8]. The Quadrotor has been sized to complete two separate flights of 37.5 nm into a headwind of 10 knots while maintaining a reserve of 20 minutes at cruise power as shown in Table 1System requirements and mission definition are detailed in Table 1 and Figure 5.

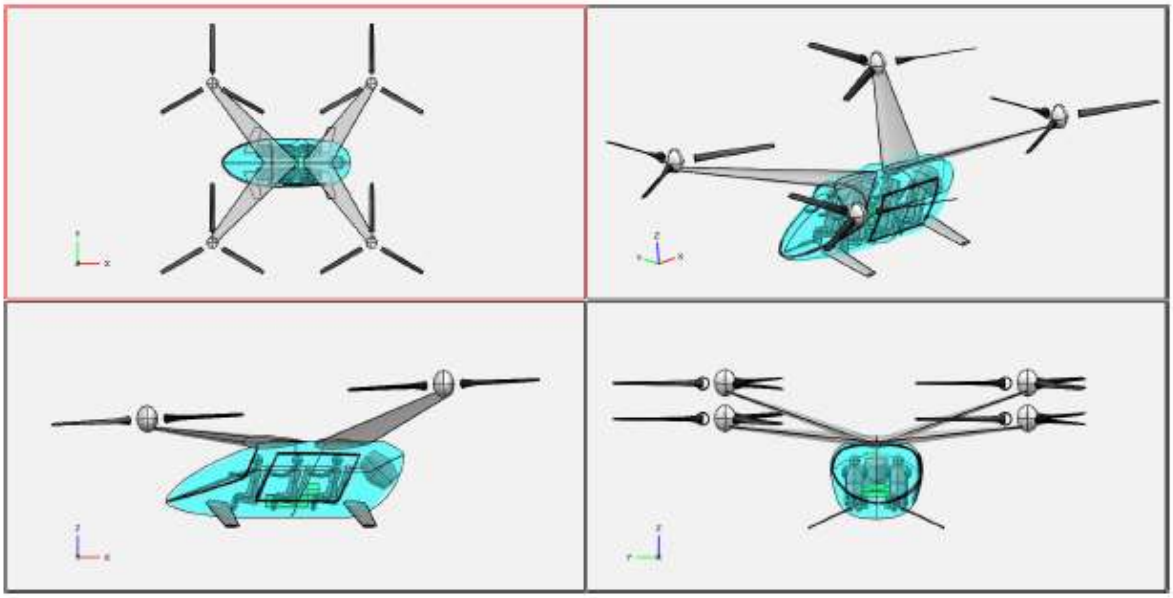

Figure 4. Six passenger quadrotor concept vehicle [3].

Table 1. Baseline and HPS engine turboshaft engine design point parameters [3].

Segment	1	2	3	4	5	6	7	8	9	10
Initial Alt. (MSL ISA)	6,000	6,000	6,050	6,050	10,000	6,050	6,050	6,050	6,000	10,000
Final Alt. (MSL ISA)	6,000	6,050	6,050	10,000	10,000	6,050	6,050	6,000	6,000	10,000
Time (sec)	15	30	10	t_{climb}	t_{cruise}	10	30	30	15	1200
Distance (nmi)	-	0	0	D_{climb}	37.5-D_{climb}	0	0	0	0	-
Speed	-	-	0	V_y	V_{br}	0	0	-	-	V_{br}
ROC (ft/min)	-	100	0	≥ 900	0	0	0	−100	-	0
Percent of Max Power	10%	100%	100%	P_{climb}	P_{cruise}	100%	100%	100%		

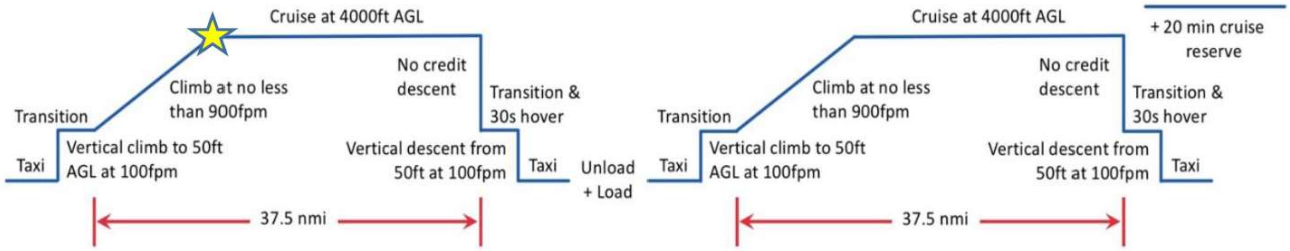

Figure 5. Six passenger quadrotor powertrain.

Sizing for this study was conducted similarly to the studies detailed within Ref. [8]. The top of climb (TOC) point, marked by the star in Figure 5, on a hot day(+27 F above international standard atmosphere conditions) was used as the sizing point for the powertrain design. The TOC point represents the largest power requirements at the most challenging environmental conditions for the powertrain. The same design point was chosen for the TMS, however the hot day assumption was increased, from +27 F to +49 F, to account for the consequences of exceeding the rated temperature and for higher temperatures at lower altitudes. The three main mission segment types (hover, climb, and cruise) are characterized by a required power setting and mission velocities as shown in Table 2. The following subsections detail the model further, with subsection A containing a description of the powertrain, subsection B showing the TMS, and subsection C reviewing the total model system integration

Table 2. Engine power requirements and velocities for the main mission point types.

Mission Segment Type	Hover	Climb	Cruise
total power demand, hp	432.0	607.0	325.4
velocity, knots	0.0	111.4	92.2

A. Powertrain Modeling

The powertrain architecture for a parallel hybrid version of the six-passenger quadrotor is a combination of the all-electric and turboshaft versions. In this architecture, four electric motors are connected to the drive shaft through gearboxes. A high-speed, low torque drive shaft connects to each rotor and ties in the turboshaft engine via another gearbox. The battery for the parallel hybrid is wired to each motor parallel to the drive shaft. This architecture drives each rotor to a constant speed and utilizes collective pitch to modulate rotor thrust. Rotor to rotor redundancy is utilized by linking all power generating devices through the drive shaft to provide protection against failures. A diagram of the final powertrain is shown in Figure 6.

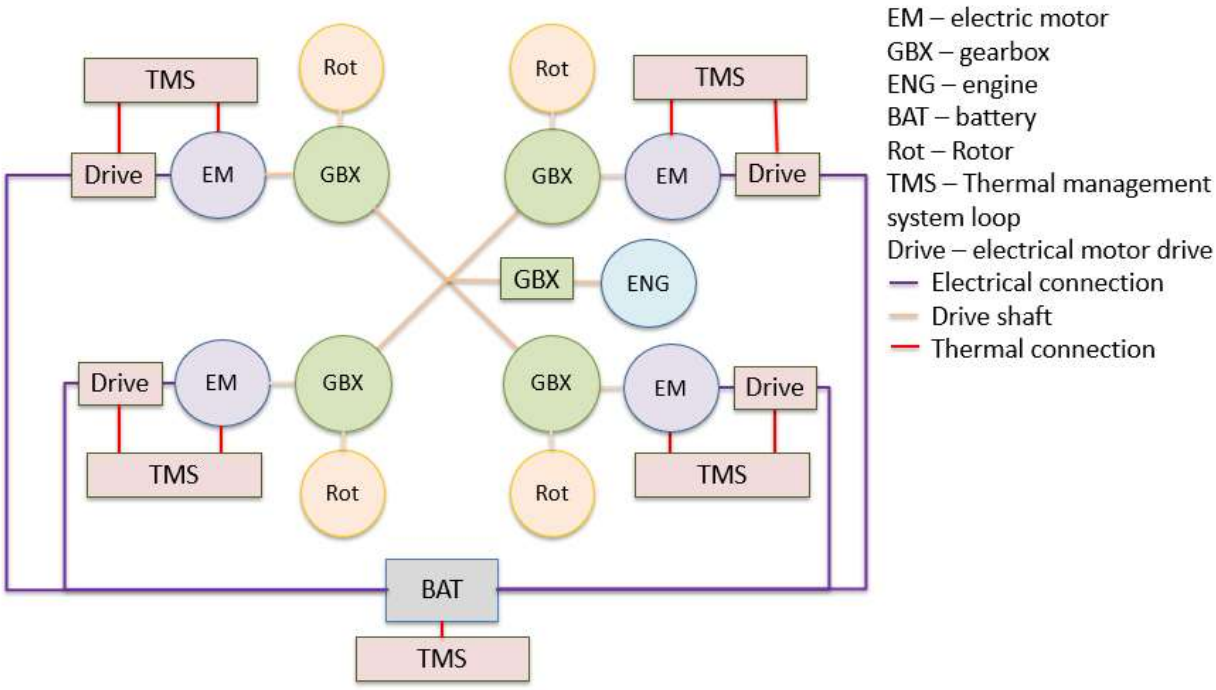

Figure 6. Six-passenger quadrotor powertrain.

Assumptions for the powertrain design are identical to those presented within Ref. [8]. Electrical system assumptions are shown in Table 3. The engine is assumed to be a single spool turboshaft that makes use of a single

stage radial compressor with a compression ratio of 8.5 Design turbine inlet temperature is assumed to be 2200 R, which is consistent with an advanced small engine with minimal cooling flow. Gas turbine weight is determined based an empirical correlation that relates weight flow to mass flow. Power demand for the system is estimated based on a momentum theory model of the rotors that follows an energy approach to calculate power from a demanded thrust and incoming air velocity [12]. This rotor model utilizes an efficiency factor that is tuned to meet thrust and power levels of the model specified in Ref. [8] developed within the NASA Design and Analysis of Rotorcraft (NDARC) tool [13]. Although this thrust is generated the powertrain simulation is run to the required power levels as described by the NDARC model.

Table 3. Powertrain specifications and assumptions [8].

Technical Specifications	Quantity
Rotor Pylon Length / Cable Length (m)	5
Hover Thrust (lbf)	1462
Climb Thrust (lbf)	1564
Design Thrust (lbf)	1564
Bus Frequency (Hz)	400
Battery Voltage (V_{dc})	1000
Battery Efficiency	0.944
Battery Specific Energy (Wh/kg)	400
Battery Hover Length (h)	1.5
Fuel Hover Length (h)	1.5
Generator Voltage (V_{ac})	1200
Electric Machine Specific Power (kW/kg)	13
Electric Machine Efficiency	0.96
Power Electronics Device Specific Power (kW/kg)	9
Power Electronics Device Efficiency	0.95
Breaker Specific Power (kW/kg)	250
Breaker Efficiency	0.995

B. Thermal Management System Model

The TMS for the electrical system components are broken up into five distinct loops, where loops that cool the electric motors and drives are located under each rotor and the battery cooling loop is located within the body of the vehicle. Design temperature limits are considered for coolant flow temperatures exiting the load and are based on values documented in Ref. [14].The maps were generated utilizing the same temperature limits and coolants as in this study.

Table 4. Component temperature limits.

Component	Electric motor	Electric motor driver	Battery*	Coolant (propylene glycol water 30%)
Temperature Limit (degrees F)	300	140	113[140]	223

* defined temperature limit is for maximum continuous power and number in brackets is a maximum short-term temperature (less than 10 minutes)

Two different TMS architectures are utilized in the system, an electric motor and driver cooling loop and a battery cooling loop. Gearbox cooling is not considered and weight for the system is assumed to be part of the gearbox weight model. The two considered cooling loops are shown in Figure 7, where inlet and nozzle elements on the air flow included. Both systems utilize a single cooling loop, an air puller fan, a single air to coolant heat exchanger (cooler), and a coolant pump. This puller fan was added to generate mass flow through the system during a hover event and reduces the overall size of the TMS. Although this system will weigh less, an air puller fan requires power to run, which increases the load on the powertrain. On the motor loop, loads were added in series to allow for lower mass flows as coolant that reaches maximum operating temperature from the driver is acceptable to run through the motor.

Additionally, this drives up the change in temperature across the heat exchanger, which makes the heat exchanger more effective.

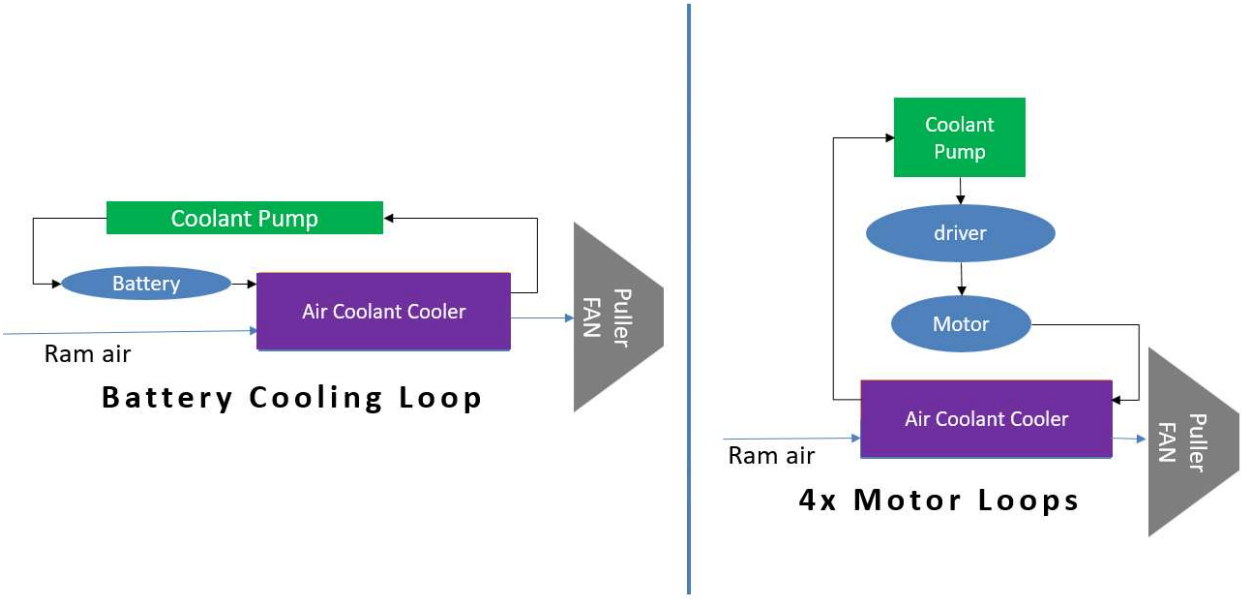

Figure 7. Six passenger quadrotor TMS loop architectures.

Sizing the system requires the use of a specialized on-design NPSS solver arrangement that is used to find mass flow, coolant flow, and heat exchanger volume at the design point. To do this, each design variable is used to meet design criterion. Coolant mass flow is adjusted to meet all temperature limits. Heat exchanger volume is adjusted to drive the heat exchanger exit temperature to equal the coolant pump input temperature, as this is a closed system. Air mass flow is then set to meet a reasonable exhaust temperature. As a guide, the exit air temperature that resulted from the optimized system (used to generate the heat exchanger maps) was selected. This temperature was 30 F greater than ambient temperature. In off-design operation, the coolant flow is held constant and air mass flow is determined in the default NPSS method where input airflow is set based on exit nozzle throat area. The coolant loop temperature is then adjusted until heat exchanger exit and coolant pump input temperatures are equal. These assumptions are consistent with a TMS that utilizes a simple control to maintain a constant coolant flow throughout the operational envelope.

C. NPSS Model Integration

There are three distinct models created within this EAP system model: engine, electrical, and thermal. During development, these models can be created independently and then integrated to complete the multidisciplinary systems analysis. To accomplish this, it is important to know which elements are performing complimentary tasks. For the electrical and engine system, this connection is made within the shaft elements through shaft ports. The engine and electrical systems are both acting on the rotor shaft. The electric motor and turbine (for a gas turbine engine) provide torque to that rotor shaft in accordance with the system's degree of hybridization or ratio of battery power to total source power. The TMS and electrical system are connected through the electrical loads and the thermal system loads, which inherit the electrical losses. This connection is made through a thermal port, but the authors found that setting the heat transfer rate within the Load itself (utilizing an NPSS pre-execute function within the thermal load element) once the electrical element has calculated is a cleaner method. During model setup it was found that creating a separate solver for the TMS also created a more stable simulation. This stability was traced to the solved heat transfer rate between the electrical components and the TMS components. Here, solving of the full EAP system would create errors in the electrical losses. These errors directly affect the solving of the TMS fluid mass flows or temperatures and created instability in the convergence of the system. Separating the TMS from the remainder of the model and solving for the TMS only after the core EAP system has converged, allows the TMS to solve using constant electrical losses, which greatly improves solving stability. A simplified integration schematic is shown in Figure 8.

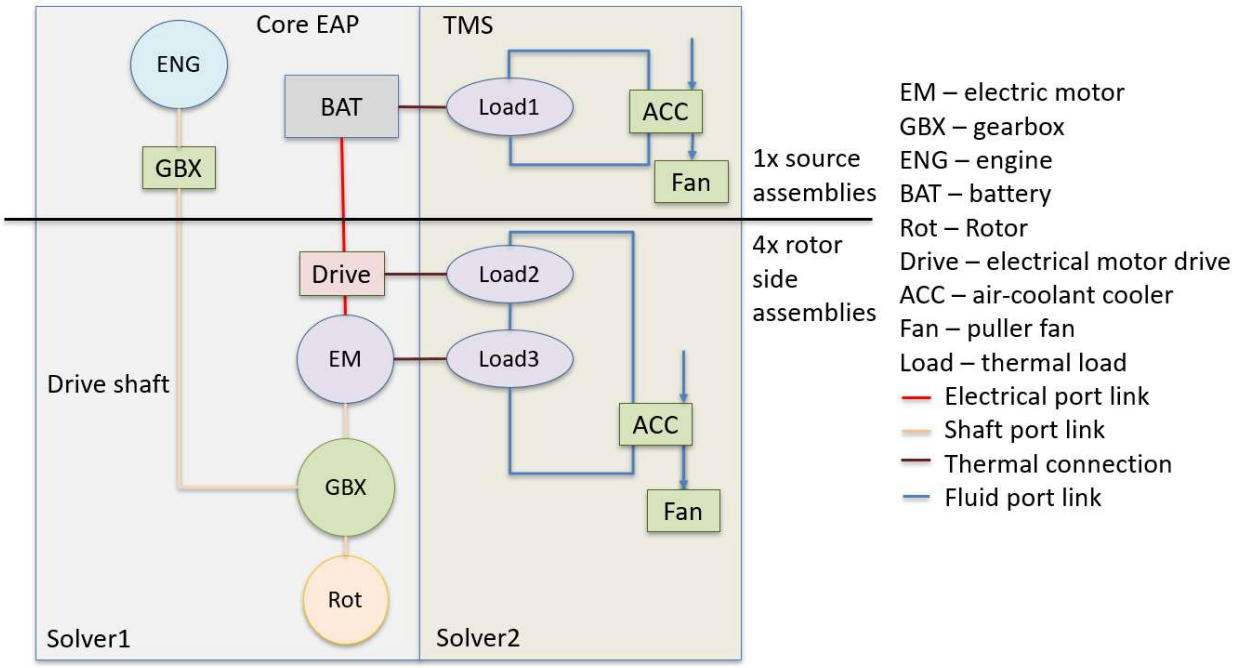

Figure 8. Quadrotor simplified EAP system integration schematic.

IV. System Design Study Results

A series of designs were completed utilizing the model detailed above. First a hybridization design sweep was completed. Hybridization was considered between 0 and 1, where 0 equates to power taken solely from the engine (all-engine) and 1 equates to power taken solely from a battery (all-electric). Fractions of hybridization result in portions of power being taken from each system, for example a 0.5 hybridization would mean that half the power comes from the engine and half from the battery at each point in the mission as described by power levels in Table 2. The second design point studies are peak systems. In the peak system, one of the power sources(engine or battery) is utilized to run only during peak conditions and the main system is designed to run at full power defined by the cruise operating point. These are designed for two configurations, where the electrical system meets the peak demand and where the engine will meet the peak demand. The third study utilizes full sized backup powertrains. In the backup study the vehicle carries a fully operational engine and electrical system with the capability of taking over for the "main" system if it should fail. In this configuration the main is utilized for the entire mission. Fuel or battery for the 20-minute reserve is then included for the secondary system. Note, for the backup configurations, reserve fuel or battery for the main system is not included for the design. It is assumed that any required reserve mission would be completed by the backup system. The backup tests are designed to analyze the effect of using a full backup powertrain without requiring duplicate power sources (fuel or battery). It is unclear if this type of arrangement would be acceptable during certification, however the case is analyzed to gain a basic understanding of what this type of system might look like. Finally, a design power sensitivity study is performed that considers performance metrics with adjustments in system power needs. These designs are summarized in Table 5. An analysis of the TMS temperatures for the all-electric configuration is in sub-section A and results of the configuration studies is in B.

Table 5. Baseline and HPS engine turboshaft engine design point parameters

Study	Description
Hybridization	System is designed to utilize different ratios of engine system and electrical system throughout the mission, 0 – all engine 1- all electrical (example 0.5 utilizes 50% engine and 50% electrical)
Peaker electrical system	Engine power system is designed for cruise and an electrical system is utilized to provide power when higher load is required.
Peaker engine system	Electrical power system is designed for cruise and an engine system is utilized to provide power when higher load is required.
Electrical backup	Engine power system is designed for the full mission without the 20-minute reserve. A full electrical backup power system is designed with enough battery to complete the 20-minute reserve.
Engine backup	Electrical power system is designed for the full mission without the 20-minute reserve. A full engine backup power system is designed with enough fuel to complete the 20-minute reserve.
Design power sensitivity	A hybridization study is completed as above for power demands as a % of the default demanded power and applied through each power request for the mission profile.

A. TMS mission point study

In the development of these conceptual models, a design point was used based on maximum power demand for the sizing of the TMS, however operational conditions such as air temperature and air flow change throughout the mission. It is therefore necessary to analyze other mission points to verify the TMS is maintaining adequate cooling for the system. Here a single loop cooling system is reviewed that utilizes a constant coolant flow rate. This architecture shows promise because it is simple, would not require modulating control system hardware, and could be controlled with an on-off scheme. Results for the all-electric configuration are located in Figure 9. Here it can be seen that the air mass flow is lowest for the design point and hover, where a puller fan is used for air circulation. For climb and cruise, the puller fan is turned off and mass flow increases with the velocity of the vehicle. Coolant mass flow was set to be constant for the mission. Design point temperature limits were set according to Table 4. Looking at the temperatures for the hover, climb, and cruise it can be observed that none of the temperatures exceed the design values. The lowest temperatures are achieved at the cruise point, where the coolant reaches a temperature of 85 F. This temperature is acceptable for this application, however the designs for this study were all completed at a hot day temperature of (+27 F). Given these low temperatures, it is advisable to run a cold day mission point as well to verify the inverter is kept to an adequate temperature. This analysis shows the considered architecture is feasible. To gain a better understanding of the system, a dynamic mission may be run that utilizes the thermal masses of the system.

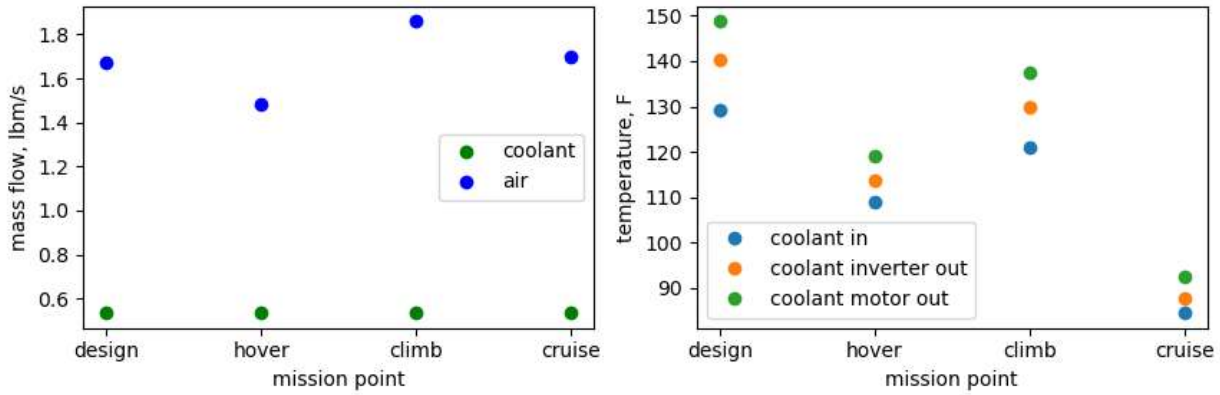

Figure 9. Mass flow rates and temperatures of the motor TMS group for the all-electric configuration at different key mission points.

B. Configuration study results

This subsection reviews results of the configuration studies listed in Table 5. In each study, the powertrain system weight is equal to the baseline vehicle's powertrain system weight, which is 2524 lbm This baseline weight includes the electrical system, fuel, TMS, battery, and gearboxes. Although this weight is constant, the amount of weight contributed by the subsystems changes for each design. An analysis of component weight is broken down in Figure 10. For this study, four main components, the gearboxes, electrical system, TMS, and the engine, were considered. Looking at each component in turn, gearbox weight changes little with changes in powertrain and is around 250 lbm. Additionally, motor to drive shaft and engine to drive shaft speeds are assumed to be similar, which results in similar mass. Engine mass is assumed to be linear, however mass estimates between hybridization levels 0.8 and 1.0 may represent prohibitively small engines and thus may not be accurate. The engine weight is roughly 350 lbm for the all-engine system. Electric system and TMS weights both increase linearly with hybridization in accordance with specific power assumptions. The electric system and TMS weigh 265 lbm and 55 lbm, respectively, for an all-electric system. Comparing engine and electric system with TMS, weights are similar for a fully electric vs. the fully engine driven. Peaker electrical and engine system designs result in near similar weights because the cruise power requirement is roughly half that of the design power requirement. The backup system weight is roughly 300 lbm higher than that of other systems. Full backup system weights for each system range from 640 lbm to 740 lbm for all except full backup system, which weighs 1020 lbm.

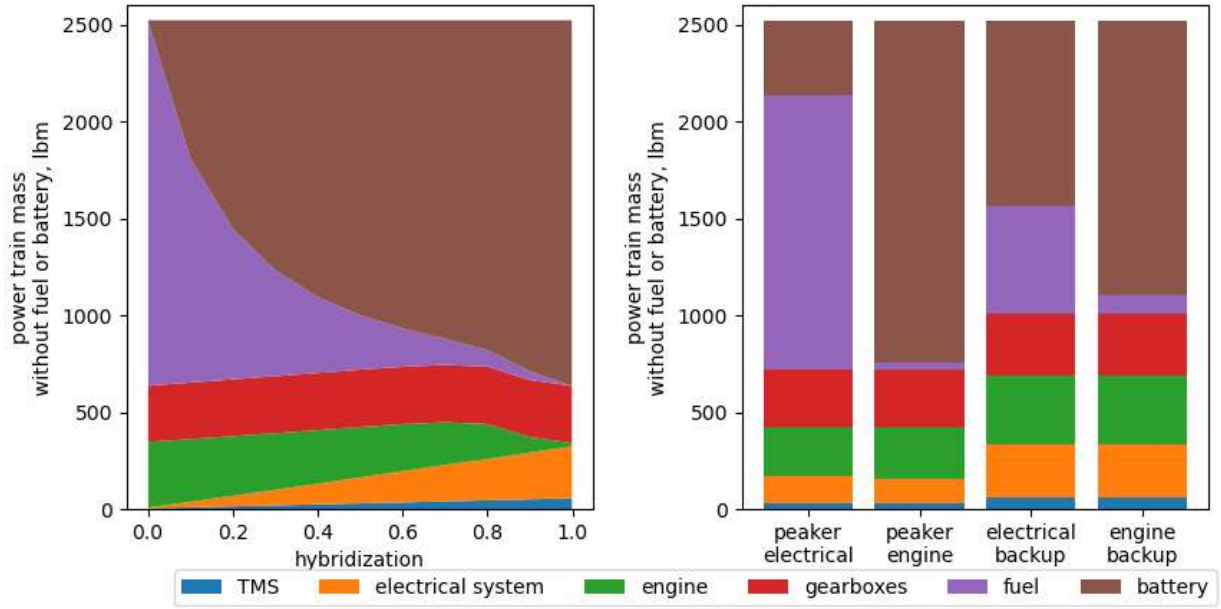

Figure 10. Powertrain component weights.

Powertrain range is analyzed as a performance metric for these studies. Results of this analysis can be seen in Figure 11. Looking at the trace, range for the all-engine system is 280 nm, much higher than the 32.5 nm range of the all-electric system. The energy density of the fuel versus that of the battery is the cause of this drop. Note, the NDARC all-electric system that this study is based on has a range of 37.5 nm. This difference can be accounted for by changes in electrical system architecture, TMS design, and inclusion of inverter efficiency. Neglecting the TMS system weight results in an estimated range of 33.7 nm for the all-electric version, , and if the TMS is neglected the estimated range would be 33.8 nm, about a 4% over estimation. Looking at the peaker electrical system, it has a range of 270 nm, slightly less than that of the all-engine system. The peaker engine and engine backup systems both increase the ranges of the all-electric system, to 33.5 nm and 33 nm, respectively. Adding an electric backup to the all-engine system results in a range of 83 nm. Engine SFC for these designs increase with hybridization as the engine size is decreased. Hybridization greater than 0.9 results in PSFC values greater than 0.8. Peaker electrical and engine systems obtain a PSFC of 0.65 lbm/hr/hp, lower than the engine version, where an SFC of 0.62 lbm/hr/hp is achieved. In this case it may be necessary to consider an alternative engine type if the configuration is to be pursued as engines of this size are inefficient. The peaker engine and engine backup studies highlight the advantages of including traditional engines

within mostly electrical configurations, as they have a range benefit compared with the all-electric system. Additionally, the all-electric with engine backup system offers redundancy advantages.

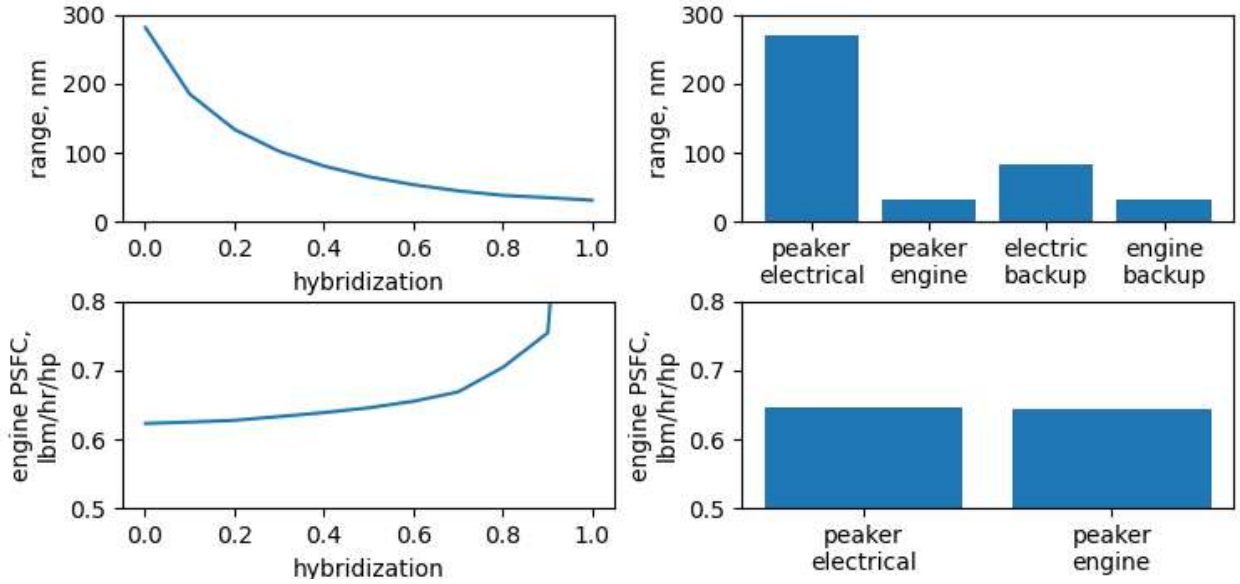

Figure 11. Vehicle range and engine design point SFC.

In electrical systems battery C-rate is a major design factor. This term characterizes how fast the battery will be required to charge or discharge and a C-rate of 1 means that the battery will discharge in 1 hour. The maximum required discharge C-rate for each design is in Figure 12. The largest observed C-rate (3.4) was with the peaker electrical configuration. Here the battery is used only to augment engine power, so the battery size is relatively small. This is followed by the electric backup configuration. Like the peaker electrical configuration, this electric backup utilizes only enough power to run the motors for 20 minutes, which leads to a C-rate of 3. The engine backup C-rate is 2.0, which is higher than the all-electric (1.75) because the reserve battery is removed. The peaker engine C-rate is 0.95, which is lower than the all-electric configuration because the engine will be used to reduce the peak power output. It can also be seen that C-rate rises with hybridization. This rise is due to the increased range and operational run time.

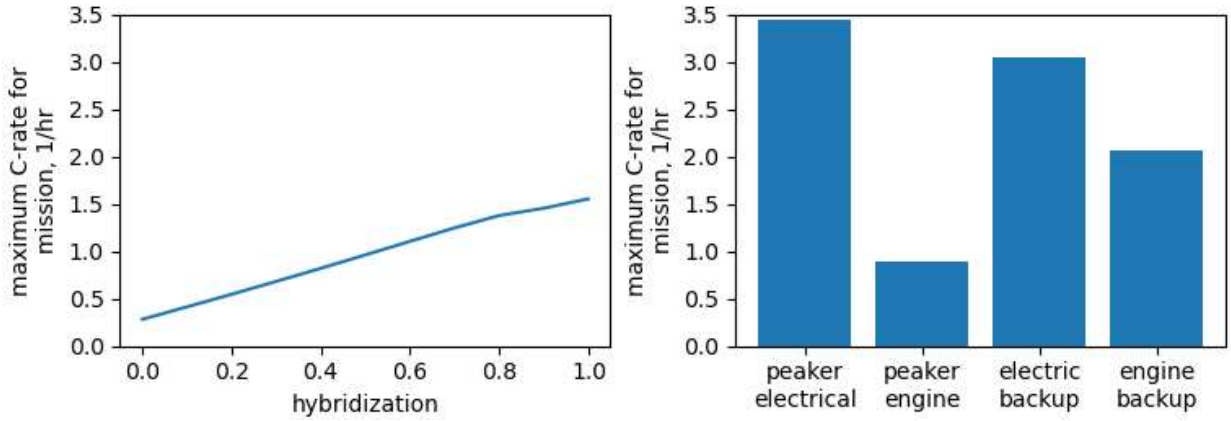

Figure 12. Battery C-rate.

In developing a conceptual vehicle model, one of the most significant metrics for the powertrain is the contributed weight. A sensitivity study was completed to determine weight with reducing or increasing power requirement. This power requirement change could come from many different factors such as, changes in aerodynamics of the vehicle, gross system weight, rotor performance, or updates in mission objective. Results of this weight study are in Figure 13. Here it can be seen that weight is increased linearly with increasing power requirement. This is to be expected because many of the weight models utilize specific power for calculation. The maximum weight observed is 790 lbm with a 10% increase in design power and the lowest is 680 lbm with a 10 % decrease in design power. Similarly, the all-electric configuration is 690 lbm (10% increase in power) and 575 lbm (10% decrease in power) and the all-engine version is 675 lbm and 590 lbm, respectively.

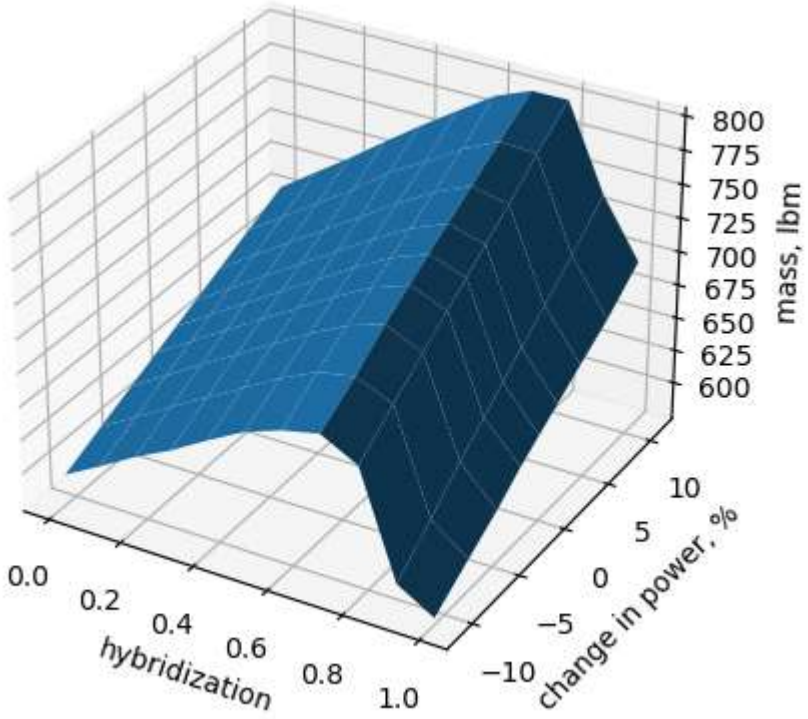

Figure 13. System weight without battery or fuel as a function of change in power and hybridization.

A similar study was completed for range. Results are shown in Figure 14. Here it can be seen that range increases with decreases in required power. As such the all-electric configuration ranges from 25nm at with 10% higher required power to 40 nm with 10% lower required power. Similarly, the all-engine configuration ranges from 247 nm (10% higher required power) to 322 nm (10% lower required power). It can be observed that the change in the all-electric version is linear with changes in required power. The all-engine version also increases range with reduction in power requirement, however the rate also decreases with that reduction in required power. This is caused by reductions in engine PSFC as the engine size is reduced.

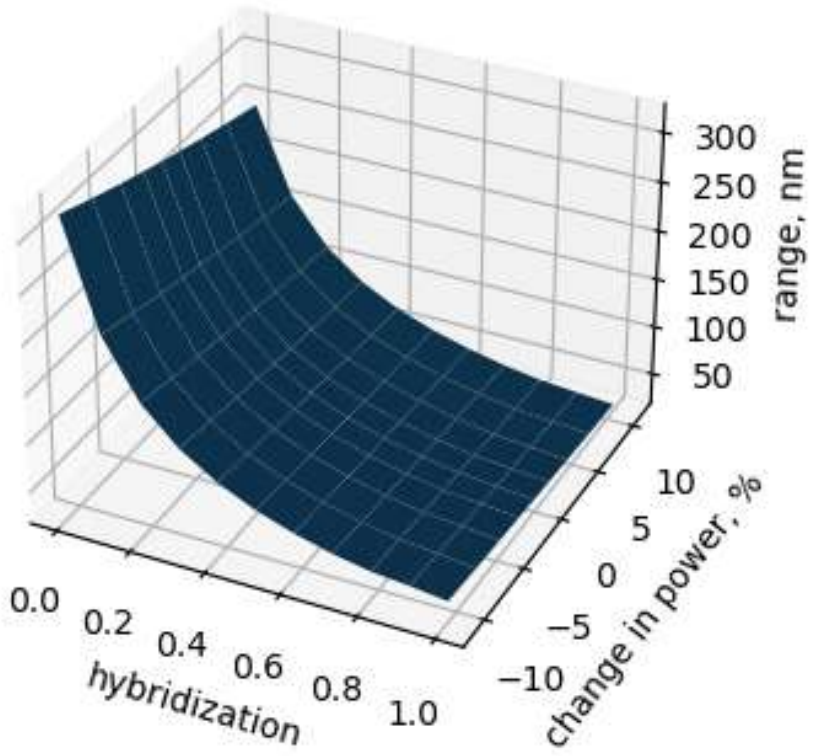

Figure 14. System weight without battery or fuel as a function of change in power and hybridization.

V. Summary and Conclusions

This paper lays out the techniques for creating and integrating a TMS into a multidisciplinary EAP system simulation, that includes an electrical system and engine system, and utilizes the NPSS software package. These techniques include updated NPSS elements developed within this paper such as performance map-based heat exchanger models and simulation development techniques, NPSS solver setup recommendations and multidisciplinary model integration methods. Utilizing these methods, a parallel-hybrid EAP system simulation for a six-passenger quadrotor is developed. This model is then used to explore several operational and design configurations. These configurations include: a percent hybridization study, a peaker engine and electrical system power reduction study, and an alternate powertrain reserve/backup study. These studies hold EAP system weight constant and adjust the mission range to reflect changes in fuel or battery size and system efficiencies. Results show that an all-engine system results in the longest vehicle range at 280 nm. Introducing an electric system and sizing the engine for cruise operation only reduces the range due to the high weight of the battery. The all-electric system results in the lowest range at 32.5 nm. Including an engine system for contributing at power levels greater than cruise results in a greater range than the all-electric at 33.5 nm. Also, including a backup engine driven power system to be utilized only during the reserve mission results in range of 33 nm. These configurations demonstrate the advantages of including an engine system onto a vehicle that is mostly electric. A final study explores a TMS architecture that utilizes a passive coolant method and shows that maintaining constant coolant flow and allowing air flow to modulate naturally is a feasible option for TMS design.

Acknowledgments

The authors would like to thank the NASA Revolutionary Vertical Lift Technology (RVLT) Project, under the Advanced Air Vehicles Program (AAVP) for the funding of this work.

Appendix

Example AUqVol heat exchanger maps shown as contours shown in Figure 15. Here AUqVol1 utilizes the coolant propylene glycol 30% and water, and AUqVol2 utilizes air.

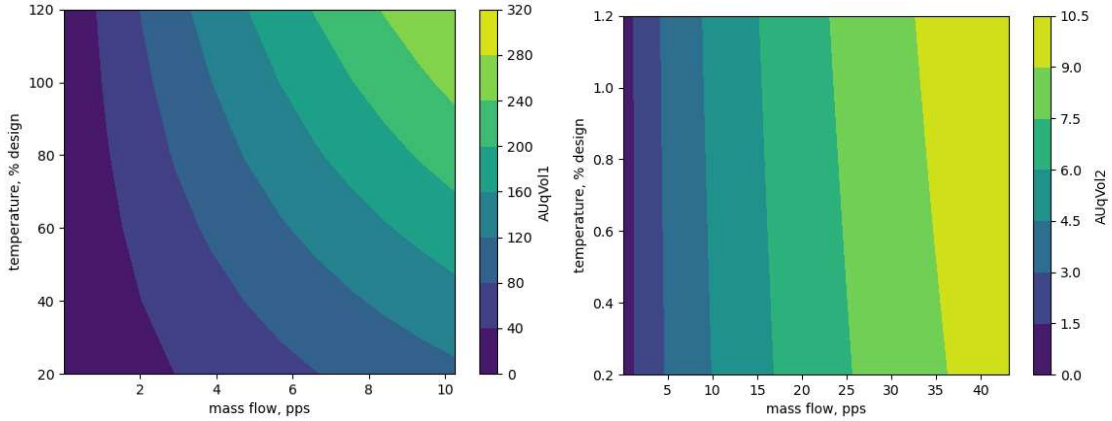

Figure 15. Heat exchanger AUqVol maps.

Example heat exchanger map in NPSS format:

```
// ********************************************************************************************
// This heat exchanger Map is a metamodel created from a heat exchanger designed within OpenMDAO,
// based on theory within Kays and London.
// The model utilizes air and propylene glycol water 30% as W2 and W1, respectively.
// ********************************************************************************************


Subelement ThermalHeatExchangerMap S_map{

 W1MapDes = 1.02513; // Design Mass Flow 1 Map propylene glycol water 30%, lbm/s
 W2MapDes = 4.30965; // Design Mass Flow 2 Map air, lbm/s

 T1MapDes = 1.0; // Design T1 Map
 T2MapDes = 1.0; // Design T2 Map

 VolDes = 0.64684; // Design volume in ft**3

 dP1Des = 2.11884; // Design dP1 in psi
 dP2Des = 0.00902; // Design dP2 in psi

 AUqVol1Des = 40.35458; // Design AUqVol1 in Btu/(s*R)/m**3
 AUqVol2Des = 3.00147; // Design AUqVol2 in Btu/(s*R)/m**3

 sWeight = 45.39939; // specific weight lbm/ft**3

 Table TB_AUqVol1(real W, real T) {
  T = 0.2000{
   W = {0.0103 , 0.1230 , 0.2358 , 0.3485 , 0.4613 , 0.5741 , 0.6868 , 0.7996 , 0.9124 , 1.0251 , 1.1276 , 2.0400 , 2.9524 , 3.8647 ,
4.7771 , 5.6895 , 6.6018 , 7.5142 , 8.4266 , 9.3389 , 10.2513 }
    AUqVol1 = {0.252 , 2.404 , 4.326 , 6.151 , 7.909 , 9.618 , 11.286 , 12.919 , 14.522 , 16.098 , 17.509 , 29.372 , 40.313 , 50.588 ,
60.338 , 69.655 , 78.605 , 87.237 , 95.592 , 103.700 , 111.589 }
  }
  T = 0.4000{
   W = *;
    AUqVol1 = {0.347 , 3.300 , 5.932 , 8.423 , 10.819 , 13.142 , 15.404 , 17.614 , 19.780 , 21.905 , 23.805 , 39.666 , 54.142 , 67.627
, 80.343 , 92.436 , 104.008 , 115.137 , 125.885 , 136.298 , 146.417 }
  }
  T = 0.6000{
```

```
  W = *;
   AUqVol1 = {0.449 , 4.271 , 7.667 , 10.872 , 13.947 , 16.921 , 19.812 , 22.631 , 25.387 , 28.087 , 30.497 , 50.481 , 68.547 ,
85.265 , 100.955 , 115.826 , 130.024 , 143.659 , 156.814 , 169.554 , 181.933 }
  }
  T = 0.8000{
   W = *;
   AUqVol1 = {0.557 , 5.284 , 9.470 , 13.411 , 17.183 , 20.823 , 24.353 , 27.788 , 31.141 , 34.420 , 37.341 , 61.425 , 83.021 ,
102.902 , 121.498 , 139.089 , 155.868 , 171.973 , 187.512 , 202.567 , 217.202 }
  }
  T = 1.0000{
   W = *;
   AUqVol1 = {0.660 , 6.248 , 11.184 , 15.818 , 20.244 , 24.505 , 28.630 , 32.638 , 36.542 , 40.355 , 43.748 , 71.575 , 96.371 ,
119.114 , 140.348 , 160.415 , 179.552 , 197.925 , 215.662 , 232.858 , 249.588 }
  }
  T = 1.2000{
   W = *;
   AUqVol1 = {0.761 , 7.198 , 12.867 , 18.177 , 23.236 , 28.098 , 32.796 , 37.353 , 41.787 , 46.109 , 49.952 , 81.332 , 109.150 ,
134.601 , 158.336 , 180.764 , 202.156 , 222.709 , 242.564 , 261.830 , 280.591 }
  }
 }

 Table TB_AUqVol2(real W, real T) {
  T = 0.2000{
   W = {0.0431 , 0.5172 , 0.9912 , 1.4653 , 1.9393 , 2.4134 , 2.8875 , 3.3615 , 3.8356 , 4.3097 , 4.7406 , 9.0024 , 13.2642 , 17.5259
, 21.7877 , 26.0495 , 30.3112 , 34.5730 , 38.8348 , 43.0965 }
   AUqVol2 = {0.222 , 0.888 , 1.274 , 1.581 , 1.846 , 2.082 , 2.298 , 2.498 , 2.686 , 2.862 , 3.016 , 4.276 , 5.271 , 6.120 , 6.873 ,
7.556 , 8.186 , 8.772 , 9.322 , 9.842 }
  }
  T = 0.4000{
   W = *;
   AUqVol2 = {0.225 , 0.899 , 1.290 , 1.601 , 1.869 , 2.108 , 2.327 , 2.529 , 2.719 , 2.898 , 3.053 , 4.328 , 5.335 , 6.195 , 6.956 ,
7.647 , 8.284 , 8.876 , 9.433 , 9.959 }
  }
  T = 0.6000{
   W = *;
   AUqVol2 = {0.228 , 0.910 , 1.306 , 1.621 , 1.892 , 2.134 , 2.355 , 2.560 , 2.752 , 2.933 , 3.090 , 4.380 , 5.399 , 6.268 , 7.038 ,
7.737 , 8.380 , 8.979 , 9.542 , 10.074 }
  }
  T = 0.8000{
   W = *;
   AUqVol2 = {0.231 , 0.921 , 1.321 , 1.640 , 1.914 , 2.159 , 2.383 , 2.590 , 2.784 , 2.968 , 3.126 , 4.431 , 5.461 , 6.339 , 7.118 ,
7.824 , 8.475 , 9.080 , 9.649 , 10.186 }
  }
  T = 1.0000{
   W = *;
   AUqVol2 = {0.233 , 0.932 , 1.336 , 1.659 , 1.936 , 2.184 , 2.410 , 2.620 , 2.816 , 3.001 , 3.162 , 4.481 , 5.522 , 6.410 , 7.197 ,
7.910 , 8.567 , 9.179 , 9.753 , 10.296 }
  }
  T = 1.2000{
   W = *;
   AUqVol2 = {0.236 , 0.942 , 1.351 , 1.677 , 1.958 , 2.208 , 2.437 , 2.649 , 2.847 , 3.035 , 3.197 , 4.530 , 5.582 , 6.479 , 7.274 ,
7.995 , 8.659 , 9.276 , 9.856 , 10.404 }
  }
 }

 Table TB_dP1(real W1) {
  W1 = {0.0103 , 0.1230 , 0.2358 , 0.3485 , 0.4613 , 0.5741 , 0.6868 , 0.7996 , 0.9124 , 1.0251 , 1.1276 , 2.0400 , 2.9524 , 3.8647
, 4.7771 , 5.6895 , 6.6018 , 7.5142 , 8.4266 , 9.3389 , 10.2513 }
  dP1 = {0.00037 , 0.03919 , 0.13332 , 0.27820 , 0.47146 , 0.71152 , 0.99717 , 1.32745 , 1.70157 , 2.11884 , 2.53514 , 7.73689 ,
15.51411 , 25.75420 , 38.37934 , 53.33038 , 70.55975 , 90.02785 , 111.70081 , 135.54907 , 161.54650 }
 }
```

```
Table TB_dP2(real W2) {
 W2 = {0.0431 , 0.5172 , 0.9912 , 1.4653 , 1.9393 , 2.4134 , 2.8875 , 3.3615 , 3.8356 , 4.3097 , 4.7406 , 9.0024 , 13.2642 , 17.5259
, 21.7877 , 26.0495 , 30.3112 , 34.5730 , 38.8348 , 43.0965 }
 dP2 = {0.000011 , 0.000400 , 0.001036 , 0.001838 , 0.002775 , 0.003829 , 0.004988 , 0.006244 , 0.007589 , 0.009019 , 0.010389
, 0.027012 , 0.048344 , 0.073649 , 0.102501 , 0.134614 , 0.169778 , 0.207829 , 0.248638 , 0.292098 }
 }
}
```

References

[1] *Think: Act, Aircraft Electrical Propulsion –The Next Chapter of Aviation?*, Roland Berger LTD, London, UK, Sept. 2017.

[2] Bowman, C., "Visions of the Future: Hybrid Electric Aircraft Propulsion," AIAA Aircraft Electric/Hybrid-Electric Power & Propulsion Workshop, July 2018.

[3] Silva, C., Johnson, W. R., Solis, E., and Patterson, M. D., , "VTOL Urban Air Mobility Concept Vehicles for Technology Development," AIAA 2018-3847, 2018 Aviation Technology, Integration, and Operations Conference, AIAA Aviation Forum, Atlanta, GA, June 25-29, 2018.

[4] Johnson, W., Silva, C., and Solis, E., "Concept Vehicles for VTOL Air Taxi Operations," AHS Specialists' Conference on Aeromechanics Design for Transformative Vertical Flight, San Francisco, CA, 2018.

[5] Kytle, J.K., "The Numerical Propulsion System Simulation: An Overview," NASA/TM-2000-209915, June 2000.

[6] Csank, J., Sadey, D., Thomas, G., Lavelle, T., Garcia, J., and Bergeson, J., (2019). "Electrical Power System Sizing Within the Numerical Propulsion System Simulation," AIAA 2019-4183, 2019 Propulsion and Energy Forum, Indianapolis, IN, August 19-22, 2019.

[7] "nasa/NPSS-Power-System-Library", https://github.com/nasa/NPSS-Power-System-Library, [software repository] [retrieved Jan. 2020].

[8] Thomas, G., Chapman, J., Alencar, J., Hasseeb, H., Sadey, D., Csank, J., "Multidisciplinary Systems Analysis of a Six Passenger Quadrotor Urban Air Mobility Vehicle Powertrain," AIAA 2020-3564, 2020 AIAA Propulsion and Energy Forum, Virtual Event, Aug. 24-28, 2020.

[9] Chapman, J., Schnulo, S., Nitzche, M., "Development of a Thermal Management System for Electrified Aircraft," AIAA 2020-0545, AIAA Science and Technology Forum, Orlando, FL, Jan. 6-10, 2020.

[10] Incropera, DeWitt, Bergman, Lavine, Fundamentals of Heat and Mass Transfer, 6th Ed., John Wiley & Sons, New York, NY, 2002.

[11] Kays, W.M., London, A.L., Compact Heat Exchangers, 3rd Ed., Krieger Publishing Co., Malabar, Florida, 1984.

[12] Gessow, A., Myers, G., *Aerodynamics of the Helicopter*, College Park Press, 1952.

[13] Johnson, W. R., "NDARC NASA Design and Analysis of Rotorcraft," NASA/TP-2015-218751, NASA, Moffett Field, CA, 2015.

[14] Chapman, J., Hasseeb, H., Schnulo, S., "Thermal Management System Design for Electrified Aircraft Propulsion Concepts," AIAA 2020-3571, AIAA Propulsion and Energy Forum, Virtual Event, Aug,24-28 ,2020.